

See discussions, stats, and author profiles for this publication at: <https://www.researchgate.net/publication/319167576>

Fault gouge graphitization as evidence of past seismic slip

Article in *Geology* · August 2017

DOI: 10.1130/G39295.1

CITATIONS

0

READS

65

10 authors, including:



Li-Wei Kuo

National Central University

32 PUBLICATIONS 545 CITATIONS

[SEE PROFILE](#)



Elena Spagnuolo

National Institute of Geophysics and Volcano...

48 PUBLICATIONS 159 CITATIONS

[SEE PROFILE](#)



Sheng-Rong Song

National Taiwan University

101 PUBLICATIONS 1,574 CITATIONS

[SEE PROFILE](#)



Stefano Aretusini

The University of Manchester

4 PUBLICATIONS 16 CITATIONS

[SEE PROFILE](#)

Some of the authors of this publication are also working on these related projects:



LUSILAB [View project](#)



NOFEAR [View project](#)

All content following this page was uploaded by [Li-Wei Kuo](#) on 23 August 2017.

The user has requested enhancement of the downloaded file.

Fault gouge graphitization as evidence of past seismic slip

Li-Wei Kuo^{1*}, Fabio Di Felice², Elena Spagnuolo², Giulio Di Toro^{2,3,4}, Sheng-Rong Song⁵, Stefano Aretusini³, Haibing Li⁶, John Suppe⁷, Jialiang Si⁶, and Cheng-Yen Wen⁸

¹Department of Earth Sciences, National Central University, Taoyuan 320, Taiwan

²Istituto Nazionale di Geofisica e Vulcanologia, 00143 Rome, Italy

³School of Earth and Environmental Sciences, University of Manchester, Manchester M13 9PL, UK

⁴Department of Geosciences, Università di Padova, 35122 Padua, Italy

⁵Department of Geosciences, National Taiwan University, Taipei 106, Taiwan

⁶Institute of Geology, Chinese Academy of Geological Sciences, 100037 Beijing, China

⁷Department of Earth and Atmospheric Science, University of Houston, Houston, Texas 77004, USA

⁸ Department of Material Science and Engineering, National Taiwan University, Taipei 106, Taiwan

ABSTRACT

One moderate- to large-magnitude earthquake ($M > 6$) nucleates in Earth's crust every three days on average, but the geological record of ancient fault slip at meters-per-second seismic velocities (as opposed to subseismic slow-slip creep) remains debated because of the lack of established fault-zone evidence of seismic slip. Here we show that the irreversible temperature-dependent transformation of carbonaceous material (CM, a constituent of many fault gouges) into graphite is a reliable tracer of seismic fault slip. We sheared CM-bearing fault rocks in the laboratory at just above subseismic and at seismic velocities under both water-rich and water-deficient conditions and modeled the temperature evolution with slip. By means of micro-Raman spectroscopy and focused-ion beam transmission electron microscopy, we detected graphite grains similar to those found in the principal slip zone of the A.D. 2008 Wenchuan (M_w 7.9) earthquake (southeast Tibet) only in experiments conducted at seismic velocities. The experimental evidence presented here suggests that high-temperature pulses associated with seismic slip induce graphitization of CM. Importantly, the occurrence of graphitized fault-zone CM may allow us to ascertain the seismogenic potential of faults in areas worldwide with incomplete historical earthquake catalogues.

INTRODUCTION

Fault rocks accommodate most of the slip during earthquakes (Sibson, 2003), but their record of deformation events occurring at typical seismic slip rates of ~ 1 m/s, as opposed to slow-slip and aseismic creep events, remains uncertain because of the lack of unequivocal characteristics (Cowan, 1999; Rowe and Griffith, 2015). Seismic slip is thought to be accommodated in centimeter- to submillimeter-thick slipping zones, and localized frictional sliding may trigger processes such as flash heating and melting, dehydration and decarbonation reactions, and thermal decomposition of fault rocks (Sibson, 2003; Di Toro et al., 2011). Because of the relatively high seismic slip rates at seismogenic depths, the natural slipping zone should record an abrupt and transient increase in temperature during earthquakes. Importantly, disordered organic compounds or amorphous carbonaceous material (CM) can be progressively and irreversibly transformed into stable graphite through thermally activated graphitization (Buseck and Beyssac, 2014). Therefore, the progressive increase in crystallographic order of CM associated with graphitization is widely utilized as an indicator of the maximum temperatures achieved by sedimentary and metamorphic rocks (Barker and Goldstein, 1990; Beyssac et al., 2002). Because CM is also found in natural fault zones, its graphitization may provide valuable information on earthquake mechanics (Oohashi et al., 2012).

Fault-zone graphitization has been proposed for the principal slip zone (PSZ) of the Longmenshan thrust fault that ruptured in a devastating A.D. 2008 M_w 7.9 Wenchuan earthquake in southeast Tibet (Kuo et al., 2014). According to data from the Wenchuan Earthquake Fault Scientific Drilling-1 project borehole 1 (WFSD-1), at 590 m depth, the active fault zone includes an ~ 54 -cm-thick black gouge made of quartz, feldspar, clay minerals, plus graphite and CM, surrounded by an ~ 2 -m-thick fault breccia made of quartz, feldspar, calcite, clay minerals, and CM (mainly poorly crystalline anthracite), but without graphite (Fig. 1; Li et al., 2013; Si et al., 2014). Wang et al. (2014) demonstrated that CM within the Wenchuan fault zone originated from adjacent host rocks (Late Triassic Xujiahe Formation). Kuo et al. (2014) speculated that gouge graphitization occurred within CM-bearing fault gouges during the 2008 M_w 7.9 Wenchuan earthquake. However, it remained unclear the process responsible for CM graphitization, under which ambient and deformation conditions it occurred, and, more relevant, if CM graphitization could be associated only with seismic slip. These crucial questions are addressed here, where we also demonstrate that the experimental products obtained at seismic slip rates are almost identical to those found in the PSZ of the Longmenshan fault, making CM graphitization a powerful tool to investigate the seismogenic potential of active faults, especially if cropping out in areas with incomplete historical earthquake catalogues.

EXPERIMENTAL METHODS

To investigate the graphitization process of the CM-bearing materials, we sheared with the rotary-shear machine SHIVA (Di Toro et al., 2010; Niemeijer et al., 2011) the graphite-free rocks of the fault breccia retrieved from 589.32 m depth. The bulk fault breccia was gently pulverized down to < 250 μm in size and poured into a ring-shaped metal sample holder designed for confinement of non-cohesive materials (Smith et al., 2012). The gouges were sheared for 3 m of slip at equivalent slip rates, V , of 0.0003 m/s (simulating just above subseismic, referred as subseismic hereafter) and 3 m/s (seismic) under a normal stress of 8.5 MPa. The experiments were conducted on 5 g of gouges (corresponding to an initial thickness of ~ 3 mm) at room temperature and humidity and, by the addition of 0.5 g of distilled water, at water-dampened conditions. Deformed samples were collected for microanalytical investigations including micro-Raman spectroscopy, field-emission scanning electron microscopy (FESEM), and focused ion beam–transmission electron microscopy (FIB-TEM) with energy dispersive X-ray spectroscopy (EDS). The natural materials of the active fault zone (black gouge and breccia) were investigated with micro-Raman spectroscopy and compared with the experimental products (Fig. 1).

RESULTS

The mechanical data, consistent with previous studies (Oohashi et al., 2011; Rutter et al., 2013; Kuo et al., 2014; Kouketsu et al., 2017), resulted

*E-mail: liweikuo@ncu.edu.tw

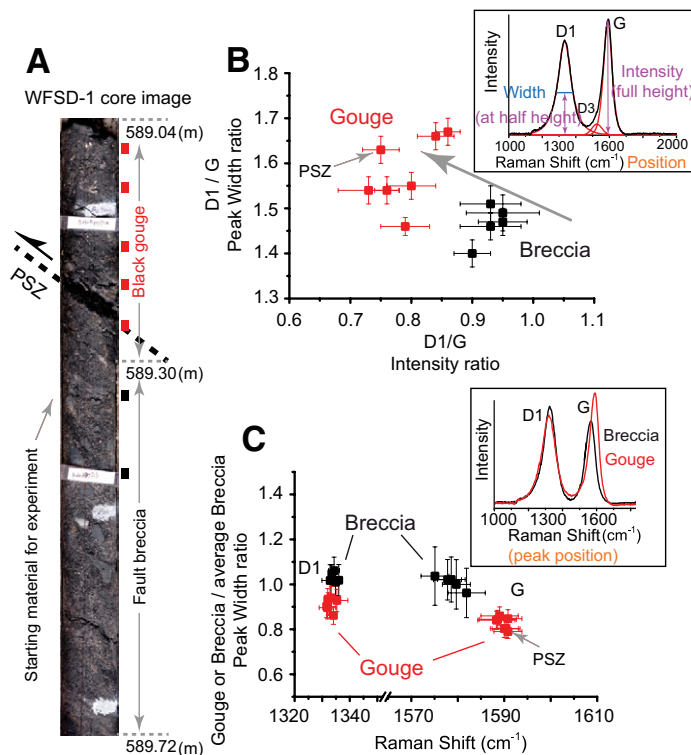


Figure 1. Wenchuan Earthquake Fault Scientific Drilling WFSD-1 borehole (southeast Tibet) core with location of studied samples and results of micro-Raman analysis. **A:** Core images exhibiting major portions of Longmenshan fault along WFSD-1 borehole. Locations of analyzed samples are indicated by red (black gouge) and black (breccia) boxes. **B:** Defect band (D1) to graphite band (G) (D1/G) peak width ratio versus D1/G intensity ratio. Inset shows representative first-order region of Raman spectrum and defines relevant spectrum decomposition parameters (width, intensity, etc.). The D3 band is attributed to out-of-phase defects. **C:** Ratio of D1 or G peak width of gouge to average breccia peak width versus G band peak position. Inset shows systematic shift toward higher frequencies of G band observed in black gouge with respect to fault breccia. PSZ—principal slip zone.

in two slip velocity–dependent behaviors (Fig. 2; Item DR2 in the GSA Data Repository¹). When sheared at seismic slip rates ($V = 3$ m/s), the experimental gouges showed pronounced weakening, with the apparent friction coefficient (defined as the ratio of shear stress to normal stress) decaying, in the room-humidity experiments, from a peak value of 0.50 to a minimum value of 0.20, and in the water-dampened experiments, from 0.18 to 0.02 (the latter had a quite complicated evolution of the friction coefficient, with minimum friction followed by re-strengthening up to 0.2 after 0.5 m and 0.25 after 2.3 m of slip). In contrast, when the gouges were sheared at subseismic slip rates ($V = 0.0003$ m/s), the effective friction coefficient evolved with slip from an initial value of 0.40 up to ~ 0.55 under room-humidity conditions, and from 0.26 to 0.37 under water-dampened conditions. The temperature evolution with slip was modeled with COMSOL Multiphysics software (<https://www.comsol.com>) using the measured frictional power dissipation (product of shear stress with slip rate) and the thermal properties of the WFSD fault gouge (Item DR3; Li et al., 2015). The initial temperature for the modeling was set to 25 °C. In the slipping zone of the gouge layer sheared under room-humidity conditions at 3 m/s (experiment s1108; seismic, RH in Fig. 2), the modeled temperature rose from 25 °C to ~ 200 °C after 0.5 m of slip, and further increased up to ~ 300 °C by the end of the experiment. Instead, under water-dampened

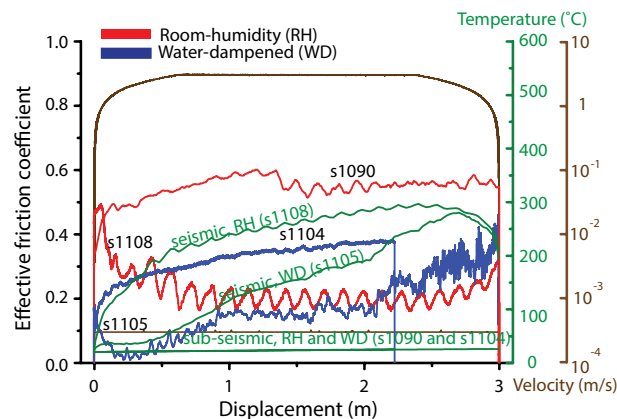


Figure 2. Experiments performed with rotary machine SHIVA on carbonaceous material (CM)-bearing materials from Longmenshan fault, southeast Tibet. Effective friction coefficient (shear stress / normal stress) versus displacement is shown for four experiments (Item DR2 [see footnote 1]) performed under room humidity (experiments s1090 [0.0003 m/s] and s1108 [3 m/s]) and water-dampened (s1105 [3 m/s] and s1104 [0.0003 m/s]) conditions. Modeled temperature evolution with slip in slipping zones obtained with COMSOL Multiphysics software (www.comsol.com) is shown for experiments all four experiments (green curves). Slip velocity curves for all experiments are shown in brown.

conditions (s1105; seismic, WD in Fig. 2), the temperature increased up to ~ 50 °C after 0.5 m of slip and progressively to ~ 280 °C until the sample was decelerated and the experiment completed. The modeled temperature in the gouges sheared at subseismic slip rates ($V = 0.0003$ m/s) was ~ 26 °C independent of the presence of liquid water (Fig. 2).

In Raman spectroscopy, the peak parameters of the D1 (defect) band and the G (graphite) band are commonly used as a gauge to quantify the degree of the graphitization process (Beysac et al., 2002, 2003) (Fig. 1B, inset; Item DR4). Here the ratio of D1 to G peak width was compared with the ratio of D1 to G peak intensity. The ratio of D1 to G peak width of either starting material (i.e., gouges) or fault breccia, normalized with the average peak width of the fault breccia, was compared to peak position (i.e., Raman shift). We analyzed five fault breccia samples, seven black gouge samples (including the PSZ of the 2008 Wenchuan earthquake), one starting material (fault breccia), and four experimental products, the latter obtained under a range of deformation conditions (Items DR5 and DR6).

The black gouge samples, compared to the fault breccia, have a lower D1/G peak intensity ratio and higher D1/G peak width ratio (Fig. 1B). Although fault breccia and black gouge have similar D1 band position and peak width ratio (Fig. 3B). Variations occur in the G band position and peak width ratio, comparing sheared samples with starting material (Fig. 3B). In the sheared materials, the G band position is shifted to higher wavelength numbers independent of slip rates.

Independent of the imposed slip rates and the presence of liquid water, the sheared gouges have a lower D1/G peak intensity ratio and higher D1/G peak width ratio with respect to the starting materials (Fig. 3A). Both starting materials and deformed gouges have a similar D1 band position and peak width ratio (Fig. 3B). Variations occur in the G band position and peak width ratio, comparing sheared samples with starting material (Fig. 3B). In the sheared materials, the G band position is shifted to higher wavelength numbers independent of slip rates.

Strain localization in the gouge layers occurred during rock deformation experiments at both subseismic and seismic rates in both wet and room-humidity conditions, developing an experimental PSZ (Figs. 4A and 4B). Volumes of the slipping zones that underwent the highest degree of strain localization were investigated with FIB-TEM-EDS and selected area electron diffraction. Starting materials and gouges sheared at subseismic slip rates had amorphous carbon (i.e., no graphite) and similar disordered regions of ~ 1 – 200 nm in size (Fig. 4C). On the contrary, gouges sheared at seismic slip rates had perfectly stacking layers (lattice spacing of $d_{002} \sim 3.55\text{Å}$) in

¹GSA Data Repository item 2017329, Items DR1–DR6 (summary of experiments, methods, and results), is available online at <http://www.geosociety.org/datarepository/2017/> or on request from editing@geosociety.org.

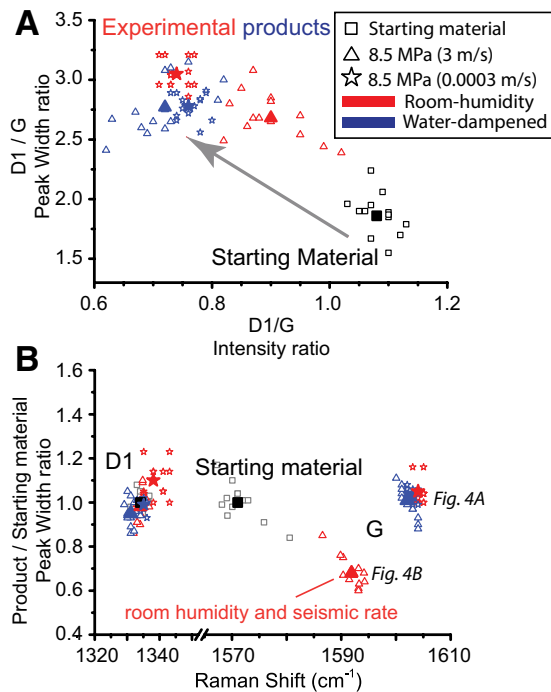


Figure 3. Raman spectra analysis of gouges sheared in rock friction experiments. **A:** Defect band (D1) to graphite band (G) (D1/G) peak width ratio versus D1/G intensity ratio. **B:** D1 or G peak widths of sheared gouges, normalized by average starting material peak widths, versus D1 or G band peak position. Two representative experimental products were selected for microstructural analysis (see Fig. 4).

defect-free carbon-built grains with ordered structures, suggesting that amorphous carbon was transformed into graphitic carbon (Fig. 4D; Item DR1).

DISCUSSION AND CONCLUSION

Amorphous CM usually contains two types of electronic configuration of carbon atoms: sp^3 or diamond like, and sp^2 or graphite like. The conversion of sp^3 -bond carbon into sp^2 -bond carbon results in graphitization of CM and in the transformation of the sp^2 -bond carbon into graphite (Ferrari and Robertson, 2000). It is well established that the D1/G peak intensity ratio is inversely proportional to the average size of the sp^2 clusters from conversion of sp^3 bonds (Fig. 3A; Ferrari and Robertson, 2000). In addition, the G band shifts toward higher frequencies in the gouges sheared at both subseismic and seismic slip rates (Fig. 3B). Therefore, the Raman spectra on experimental products show that the transformation of sp^3 -bond carbon into sp^2 -bond carbon in the amorphous carbon network was driven by bulk shear strain, suggesting rehybridization of interacting dangling bonds of carbon during both subseismic and seismic slip (Pastewka et al., 2011).

Heating has been suggested to order phases of sp^2 and result in the formation of graphite from clusters of carbon atoms (Thomas et al., 2006), determining a smaller G band peak width (Beyssac et al., 2002). In the experiments performed on gouges at seismic slip rates and room-humidity conditions, high temperatures (up to 300 °C) were achieved during frictional sliding, and the small width ratio of G bands (red triangles in Fig. 3B; Fig. 4D) suggests the crystallization of carbon into graphite. By contrast, in the water-dampened experiments performed on gouges at seismic slip rates, water vaporization possibly buffered the temperature increase (limited to <200 °C) and impeded the formation of graphite (blue triangles in Fig. 3B; Chen et al., 2017). Moreover, in the experiments performed at subseismic slip rates and independent of the water content, the temperature remained at ~ 26 °C (Fig. 2). In the latter sheared gouges, the similar width ratio of both D1 and G compared to the starting materials suggest the presence of a random-order sp^2 -bond domain (Figs. 3B and 4C; Item DR1) and, therefore, the absence of graphitization processes.

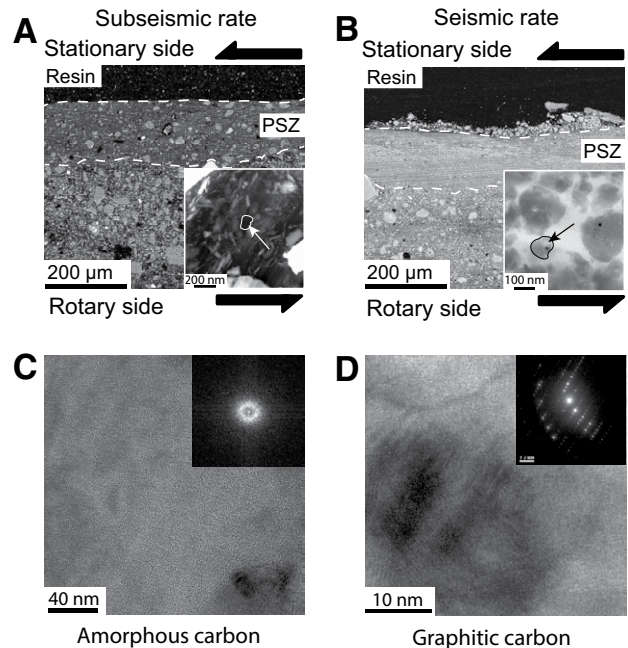


Figure 4. Microstructures in gouges sheared under room-humidity conditions at just above subseismic (experiment s1090) and seismic (experiment s1002) slip rates. **A,B:** Strain localized in principal slip zones (PSZs). Insets show presence of carbonaceous material (CM) within PSZ (field-emission scanning electron microscopy images). **C:** Poorly ordered carbon grains (see selected area electron diffraction [SAED] pattern in inset) within PSZ formed at subseismic slip rates (transmission electron microscopy [TEM] image). **D:** Well-crystallized carbon (see SAED pattern in inset) within PSZ formed at seismic slip rates (TEM image).

Our rock friction experiments demonstrate that CM graphitization is characterized by (1) decreasing D1/G peak intensity ratio, (2) shift of G peak position toward higher frequencies, and (3) smaller peak width ratio than the starting materials. The changes in the Raman spectra result from the formation of sp^2 clusters in the CM due to strain (Ross and Bustin, 1990) rather than strain rate. Instead, the decrease in G band peak width ratio, which indicates increased crystallinity of the CM, is attributed to frictional heating. As a consequence, the microstructural and/or mineralogical evolution of CM (amorphous at subseismic slip rates and reordering and graphitization at seismic slip rates) may allow us to individuate active seismogenic faults. However, the absence of evidence of graphitization processes in CM-bearing gouges (see wet experiments at seismic rates) is not indicative of aseismic behavior of the faults.

Because our experiments at seismic slip rates, and in the absence of liquid water, showed enhanced graphitization of CM (Fig. 3), we may interpret the analyses on WFSD-1 fault rocks as follows. The anti-correlation between peak width ratio and peak intensity ratio suggests that the transformation of sp^3 -bond carbon into sp^2 -bond carbon occurs within the black gouge (Fig. 1B), and a shift to high frequency of the G band from breccia to gouge is presumably due to strain (Fig. 1C). In particular, the narrower G peak width of black gouge suggests that CM contains abundant well-ordered sp^2 domains, implying that the black gouge was exposed to an increase in temperature under water-deficient conditions (Kuo et al., 2014). Permeability measurements of the WFSD-1 borehole suggested that coseismic drainage was critical for later healing the fault damage associated with seismic rupture propagation (Xue et al., 2013). It seems likely that, during seismic slip, pore fluids were expelled from the slipping zone, and seismic slip resulted in locally dry conditions allowing gouge graphitization. This hypothesis is consistent with the finding of pseudotachylytes (solidified friction melts typically associated with seismic slip under water-deficient conditions; Sibson and Toy, 2006) in the PSZ of the 2008 M_w 7.9 Wenchuan earthquake retrieved at ~ 1000

m depth from the WFSD-1 borehole (Wang et al., 2016). In addition, because water circulation was vigorous within the fault zone following the main shock (Xue et al., 2013), other chemical interactions with carbon and hydrothermal fluid at various ambient conditions must be taken into consideration (Oohashi et al., 2012; Rumble, 2014).

Importantly, the fault-zone wall rocks have lower thermal conductivity ($\sim 1 \text{ W m}^{-1} \text{ K}^{-1}$) compared to the sample metal holder ($\sim 40 \text{ W m}^{-1} \text{ K}^{-1}$; Item DR3). In nature, compared to the experiments, this should result in a higher temperature rise and longer duration of higher temperatures, favoring graphitization kinetics during seismic slip (Yao et al., 2015). However, the higher G peak width ratio of the natural gouges with respect to the gouge deformed at room-humidity conditions implies that the natural gouges were exposed to lower frictional power dissipation with respect to the experimental gouges. Coseismic fluid drainage (and water vaporization) efficiently dissipated the frictional heat generated during seismic slip, buffering the temperature increase, and therefore resulting in less temperature-induced graphitization (Fig. 1C). The micro-Raman measurements presented here are in accordance with those from the WFSD-1 borehole (Kuo et al., 2014; Si et al., 2014; Li et al., 2015) and support the interpretation that the Longmenshan fault was extremely weak during seismic slip.

Our results find application in determining seismic fault movement in general. Due to the resistance of graphitized products to alteration and weathering, the state of graphitization of CM (if graphite is related to faulting and not due to precipitation from percolating fluids, etc.) could be a suitable indicator of historical or ancient earthquakes in faults. Only low-grade amorphous CM was found in the surface rupture of the Longmenshan fault (Kouketsu et al., 2017), suggesting that gouge graphitization requires a certain amount of energy (shear stress, strain, and temperature) to be triggered (Kuo et al., 2014). As a consequence, the presence of graphite at depth ($>500 \text{ m}$) within active fault zones might be a robust indicator of seismic hazard in areas worldwide with incomplete historical earthquake catalogues.

ACKNOWLEDGMENTS

This research used materials provided by the Wenchuan Earthquake Fault Scientific Drilling program of the China National Science and Technology Planning Project. We thank John Platt and two anonymous reviewers for their positive and constructive comments, and editor Dennis Brown for his help throughout the publication process. Part of this work was supported by the National Science Foundation of China (41330211, 41520104006) to Haibing Li, the European Research Council Consolidator Starting Grant 614705 NOFEAR to Giulio Di Toro, and Taiwan ROC (Republic of China) Ministry of Science and Technology (MOST 105-2628-M-008-002-MY3) and National Central University grants to Li-Wei Kuo.

REFERENCES CITED

Barker, C.E., and Goldstein, R.H., 1990, Fluid-inclusion technique for determining maximum temperature in calcite and its comparison to the vitrinite reflectance geothermometer: *Geology*, v. 18, p. 1003–1006, doi:10.1130/0091-7613(1990)018<1003:FITFDM>2.3.CO;2.

Beysac, Q., Goffé, B., Chopin, C., and Rouzaud, J.N., 2002, Raman spectra of carbonaceous material in metasediments: A new geothermometer: *Journal of Metamorphic Geology*, v. 20, p. 859–871, doi:10.1046/j.1525-1314.2002.00408.x.

Beysac, Q., Goffé, B., Petitet, J.P., Froigneux, E., Moreau, M., and Rouzaud, J.N., 2003, On the characterization of disordered and heterogeneous carbonaceous materials by Raman spectroscopy: *Spectrochimica Acta Part A: Molecular and Biomolecular Spectroscopy*, v. 59, p. 2267–2276, doi:10.1016/S1386-1425(03)00070-2.

Buseck, P.R., and Beysac, O., 2014, From organic matter to graphite: Graphitization: *Elements*, v. 10, p. 421–426, doi:10.2113/gselements.10.6.421.

Chen, J., Niemeijer, A., Yao, L., and Ma, S., 2017, Water vaporization promotes coseismic fluid pressurization and buffers temperature rise: *Geophysical Research Letters*, v. 44, p. 2177–2185, doi:10.1002/2016GL071932.

Cowan, D.S., 1999, Do faults preserve a record of seismic slip? A field geologist's opinion: *Journal of Structural Geology*, v. 21, p. 995–1001, doi:10.1016/S0191-8141(99)00046-2.

Di Toro, G., et al., 2010, From field geology to earthquake simulation: A new state-of-the-art tool to investigate rock friction during the seismic cycle (SHIVA): *Rendiconti Lincei: Scienze Fisiche e Naturali*, v. 21, Supplement, p. 95–114, doi:10.1007/s12210-010-0097-x.

Di Toro, G., Han, R., Hirose, T., De Paola, N., Nielsen, S., Mizoguchi, K., Ferri, F., Cocco, M., and Shimamoto, T., 2011, Fault lubrication during earthquakes: *Nature*, v. 471, p. 494–498, doi:10.1038/nature09838.

Ferrari, A.C., and Robertson, J., 2000, Interpretation of Raman spectra of disordered and amorphous carbon: *Physical Review B: Condensed Matter and Materials Physics*, v. 61, p. 14095–14107, doi:10.1103/PhysRevB.61.14095.

Kouketsu, Y., Shimizu, I., Wang, Y., Yao, L., Ma, S., and Shimamoto, T., 2017, Raman spectra of carbonaceous materials in a fault zone in the Longmenshan thrust belt, China: Comparisons with those of sedimentary and metamorphic rocks: *Tectonophysics*, v. 699, p. 129–145, doi:10.1016/j.tecto.2017.01.015.

Kuo, L.W., Li, H., Smith, S., Di Toro, G., Suppe, J., Song, S.R., Nielsen, S., Sheu, H.S., and Si, J., 2014, Gouge graphitization and dynamic fault weakening during the 2008 Mw 7.9 Wenchuan earthquake: *Geology*, v. 42, p. 47–50, doi:10.1130/G34862.1.

Li, H., et al., 2013, Characteristics of the fault-related rocks, fault zones and the principal slip zone in the Wenchuan Earthquake Fault Scientific Drilling Hole-1 (WFSD-1): *Tectonophysics*, v. 584, p. 23–42, doi:10.1016/j.tecto.2012.08.021.

Li, H., et al., 2015, Long-term temperature records following the M_w 7.9 Wenchuan (China) earthquake are consistent with low friction: *Geology*, v. 43, p. 163–166, doi:10.1130/G35515.1.

Niemeijer, A.R., Di Toro, G., Nielsen, S., and Di Felice, F., 2011, Frictional melting of gabbro under extreme experimental conditions of normal stress, acceleration, and sliding velocity: *Journal of Geophysical Research*, v. 116, B07404, doi:10.1029/2010JB008181.

Oohashi, K., Hirose, T., and Shimamoto, T., 2011, Shear-induced graphitization of carbonaceous materials during seismic fault motion: Experiments and possible implications for fault mechanics: *Journal of Structural Geology*, v. 33, p. 1122–1134, doi:10.1016/j.jsg.2011.01.007.

Oohashi, K., Hirose, T., Kobayashi, K., and Shimamoto, T., 2012, The occurrence of graphite-bearing fault rocks in the Atotsugawa fault system, Japan: Origins and implications for fault creep: *Journal of Structural Geology*, v. 38, p. 39–50, doi:10.1016/j.jsg.2011.10.011.

Pastewka, L., Moser, S., Gumbsch, P., and Moseler, M., 2011, Anisotropic mechanical amorphization drives wear in diamond: *Nature Materials*, v. 10, p. 34–38, doi:10.1038/nmat2902.

Ross, J.V., and Bustin, R.M., 1990, The role of strain energy in creep graphitization of anthracite: *Nature*, v. 343, p. 58–60, doi:10.1038/343058a0.

Rowe, C.D., and Griffith, W.A., 2015, Do faults preserve a record of seismic slip: A second opinion: *Journal of Structural Geology*, v. 78, p. 1–26, doi:10.1016/j.jsg.2015.06.006.

Rumble, D., 2014, Hydrothermal graphitic carbon: *Elements*, v. 10, p. 427–433, doi:10.2113/gselements.10.6.427.

Rutter, E.H., Hackston, A.J., Yeatman, E., Brodie, K.H., Mecklenburgh, J., and May, S.E., 2013, Reduction of friction on geological faults by weak-phase smearing: *Journal of Structural Geology*, v. 51, p. 52–60, doi:10.1016/j.jsg.2013.03.008.

Si, J., Li, H., Kuo, L.W., Pei, J., Song, S.R., and Wang, H., 2014, Clay mineral anomalies in the Yingxiu–Beichuan fault zone from the WFSD-1 drilling core and its implication for the faulting mechanism during the 2008 Wenchuan earthquake (Mw 7.9): *Tectonophysics*, v. 619–620, p. 171–178, doi:10.1016/j.tecto.2013.09.022.

Sibson, R.H., 2003, Thickness of the seismic slip zone: *Bulletin of the Seismological Society of America*, v. 93, p. 1169–1178, doi:10.1785/0120020061.

Sibson, R.H., and Toy, V.G., 2006, The habitat of fault-generated pseudotachylite: Presence vs. absence of friction-melt, in Abercrombie, R., et al., eds., *Earthquakes: Radiated Energy and the Physics of Faulting*: American Geophysical Union Geophysical Monograph 170, p. 153–166, doi:10.1029/170GM16.

Smith, S.A.F., Di Toro, G., Kim, S., Ree, J.-H., Nielsen, S., Billi, A., and Spiess, R., 2012, Coseismic recrystallization during shallow earthquake slip: *Geology*, v. 41, p. 63–66, doi:10.1130/G33588.1.

Thomas, P., Delbe, K., Himmel, D., Mansot, J.L., Cadore, F., and Guerin, K., 2006, Tribological properties of low-temperature graphite fluorides: Influence of the structure on the lubricating performances: *Journal of Physics and Chemistry of Solids*, v. 67, p. 1095–1099, doi:10.1016/j.jpcs.2006.01.084.

Wang, H., Li, H., Janssen, C., and He, X., 2016, Seismic energy partitioning during the 2008 Mw 7.9 Wenchuan earthquake from WFSD-1 core sample: Abstract S33C-2850 presented at the 2016 Fall Meeting, American Geophysical Union, San Francisco, California, 12–16 December.

Wang, Y., Ma, S., Shimamoto, T., Yao, L., Chen, J., Yang, X., He, H., Dang, J., Hou, L., and Togo, T., 2014, Internal structures and high-velocity frictional properties of Longmenshan fault zone at Shenxigou activated during the 2008 Wenchuan earthquake: *Earthquake Science*, v. 27, p. 499–528, doi:10.1007/s11589-014-0096-6.

Xue, L., et al., 2013, Continuous permeability measurements record healing inside the Wenchuan earthquake fault zone: *Science*, v. 340, p. 1555–1559, doi:10.1126/science.1237237.

Yao, L., Ma, S., Platt, J.D., Niemeijer, A.R., and Shimamoto, T., 2015, The crucial role of temperature in high-velocity weakening of faults: Experiments on gouge using host blocks with different thermal conductivities: *Geology*, v. 44, p. 63–66, doi:10.1130/G37310.1.

Manuscript received 6 May 2017

Revised manuscript received 25 July 2017

Manuscript accepted 26 July 2017

Printed in USA